



Swansea University  
Prifysgol Abertawe



## Cronfa - Swansea University Open Access Repository

---

This is an author produced version of a paper published in:

*Electrochimica Acta*

Cronfa URL for this paper:

<http://cronfa.swan.ac.uk/Record/cronfa36722>

---

### **Paper:**

Liu, R., Scully, J., Williams, G. & Birbilis, N. (2017). Reducing the corrosion rate of magnesium via microalloying additions of group 14 and 15 elements. *Electrochimica Acta*

<http://dx.doi.org/10.1016/j.electacta.2017.11.062>

---

This item is brought to you by Swansea University. Any person downloading material is agreeing to abide by the terms of the repository licence. Copies of full text items may be used or reproduced in any format or medium, without prior permission for personal research or study, educational or non-commercial purposes only. The copyright for any work remains with the original author unless otherwise specified. The full-text must not be sold in any format or medium without the formal permission of the copyright holder.

Permission for multiple reproductions should be obtained from the original author.

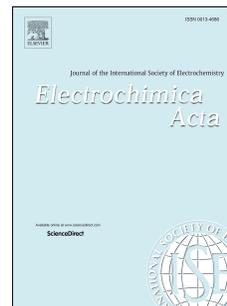
Authors are personally responsible for adhering to copyright and publisher restrictions when uploading content to the repository.

<http://www.swansea.ac.uk/library/researchsupport/ris-support/>

# Accepted Manuscript

Reducing the corrosion rate of magnesium via microalloying additions of group 14 and 15 elements

R.L. Liu, J.R. Scully, G. Williams, N. Birbilis



PII: S0013-4686(17)32413-1

DOI: [10.1016/j.electacta.2017.11.062](https://doi.org/10.1016/j.electacta.2017.11.062)

Reference: EA 30652

To appear in: *Electrochimica Acta*

Received Date: 11 August 2017

Revised Date: 9 November 2017

Accepted Date: 10 November 2017

Please cite this article as: R.L. Liu, J.R. Scully, G. Williams, N. Birbilis, Reducing the corrosion rate of magnesium via microalloying additions of group 14 and 15 elements, *Electrochimica Acta* (2017), doi: 10.1016/j.electacta.2017.11.062.

This is a PDF file of an unedited manuscript that has been accepted for publication. As a service to our customers we are providing this early version of the manuscript. The manuscript will undergo copyediting, typesetting, and review of the resulting proof before it is published in its final form. Please note that during the production process errors may be discovered which could affect the content, and all legal disclaimers that apply to the journal pertain.

<sup>1</sup>Department of Materials Science and Engineering, Monash University, Clayton, VIC 3800,  
Australia

<sup>2</sup>Department of Materials Science and Engineering, University of Virginia, Charlottesville, VA  
22904, USA

<sup>3</sup>Materials Research Centre, College of Engineering, Swansea University, Bay Campus, Crymlyn  
Burrows, Swansea, SA1 8EN, UK

\*nick.birbilis@monash.edu

+61 399054941

**Abstract:**

A characteristic of magnesium (Mg) dissolution is that dissolution is accompanied by a concomitant increase in the hydrogen evolution reaction (HER), a phenomenon known as cathodic activation. When magnesium undergoes free corrosion or forced dissolution in response to anodic polarisation, cathodic activation is manifest, which allows magnesium dissolution to readily proceed. However, recent work revealed that alloying magnesium with micro additions of arsenic, As (a group 15 element) was capable of retarding cathodic activation, resulting in a significant reduction in the corrosion rate of Mg-As alloys. As such, in the pursuit of elements with similar chemical and electrochemical properties to arsenic, but with less toxicity, a number of group 14 and 15 elements were alloyed with magnesium and reported herein. Based on the binary alloying additions studied herein, it was revealed that Bi, Ge, Pb, Sb and Sn, demonstrated suppression of cathodic activation of Mg following anodic polarisation (about one order of magnitude lower based on the cyclic galvanostatic-potentiostatic testing), in addition to lower free corrosion rates (about one order of magnitude based on the mass loss and hydrogen evolution testing). Employing a number of corrosion rate assessments, including online atomic emission spectroelectrochemistry, it was shown that reduction in Mg corrosion rates – historically considered difficult to achieve – can be robustly demonstrated. The present work has implications for the development of more corrosion resistant Mg alloys, Mg anodes for cathodic protection, or for the use of Mg as a primary battery electrode.

**Keywords:** Magnesium, Corrosion, Cathodic activation, Magnesium alloys, ICP.

in the utility of Mg as an electrode material in both primary and secondary battery systems, due to its high energy density [6, 7]. As well recognised, the inherently high rate of Mg corrosion in aqueous environments restricts the wider engineering application of Mg [1, 3, 8]. The high dissolution rate of Mg anodes at open-circuit causes “parasitic discharge” issues in primary Mg battery systems [9-11]. Thus, using appropriate approaches for controlling the corrosion of Mg is of vital importance.

Compared to common engineering metals, Mg is highly reactive in aqueous environments [1, 12]. Water reduction ( $2\text{H}_2\text{O} + 2\text{e}^- \rightarrow \text{H}_2 + 2\text{OH}^-$ ) is the primary cathodic reaction which has few kinetic limitations, such as no requirement for the presence oxygen [13]. Magnesium itself is incapable of forming a passive surface oxide/hydroxide layer in aqueous or moist environments of  $\text{pH} < 11$  [1, 12, 13], and consequently, corrosion of Mg occurs readily over a wide pH range (from about pH -2 to ~10.5) [12]. Furthermore, under anodic polarisation, the rate of partial cathodic reaction upon Mg, which is the hydrogen evolution reaction (HER), also increases substantially with increasing anodic potential. This phenomenon is termed the “negative difference effect (NDE)”, which has been documented for several decades [14-19]. The recent works of Williams and co-workers described a so-called anodically induced “cathodic activation” phenomenon, which was clarified using the scanning vibrating electrode technique (SVET) [20, 21]. The notion that cathodic (catalytic) activity is enhanced by prior anodic polarisation has also been confirmed in a variety of tests using conventional electrochemical methods [19]. In addition, cathodic activation of Mg has been found to occur in chloride containing electrolyte without any external polarisation [22]. The anodic reaction kinetics of Mg dissolution as assessed from potentiodynamic polarisation testing curve reveals a very low Tafel-slope, concomitant with the inherently non-polarisable nature of Mg [13]. As such, small changes in cathodic kinetics have a significant effect on the overall corrosion rate of Mg, and corrosion of Mg may be considered a “cathodic reaction controlled” process.

With respect to the control of Mg corrosion, either utilisation of surface protective coatings or appropriate alloying is required [23-26]. Corrosion protection of Mg by surface treatment incurs a significant cost in many cases, in addition to coatings on Mg being inherently restricted to barrier coatings that are unable to protect at defect sites. Consequently, corrosion resistant Mg alloys via alloying remain an attractive route. Unlike the improvement of mechanical properties by alloying, which is widely reported in the literature [2, 27, 28]; alloying additions generally increase the rate of cathodic reaction and anodically induced cathodic activation upon Mg, leading to more severe

[33]. The limited solid solubility of a wide range of elements in Mg [24, 27] restricts the use of appropriate alloying (to a critical concentration) required to modify the surface oxide layer properties. The exceptional case has been reported in the recent work of Xu et al. [34], wherein an Mg-10.9Li (wt.%) alloy with a body centred cubic (bcc) structure was developed. The Mg-Li alloy possessed a dynamically formed Li-rich carbonate surface film, which provided remarkable corrosion resistance [35]. However, imparting this stainless-like character to other Mg alloys with hexagonal close packed (hcp) structure via forming an inherently formed passive surface films as similar to Mg-Li alloy, is challenging [36]. Thus, the development of corrosion resistant Mg alloys via metallurgical alloying is indeed an aspect of important work.

A recent breakthrough in the development of an intrinsically corrosion resistant Mg alloy was achieved via the use of microalloying additions of arsenic (As) [37], to reduce cathodic kinetics and suppress cathodic activation, imparting remarkable corrosion resistance to Mg. However, the use of As is considered problematic in industrial manufacturing (or even laboratory testing) owing to the toxicity of As. Therefore, the pursuit of less toxic elements to control the corrosion of Mg in a manner similar to that demonstrated by Mg-As, would provide a practical corrosion control route. The corrosion protection imparted by the small concentration of metallic As relies on the ability of As species to serve as a poison for cathodic reaction and to hinder cathodic reaction and overall corrosion reaction of Mg [38, 39]. In addition, cathodic poisons are capable of effectively retarding the rate of cathodic reaction at low concentrations [40, 41]. In pursuit of elements that possess similar inherent catalytic traits with As, but with less toxicity, a number of group 14 and 15 elements including bismuth (Bi), germanium (Ge), lead (Pb), antimony (Sb), and tin (Sn) were studied herein [42, 43].

There exist several reports regarding the influence of aforementioned group 14 and 15 elements on the corrosion of Mg and Mg alloys. It was reported by Tak et al. [44] that addition of Bi (0.5-15 wt.%) deteriorated the corrosion resistance of Mg-1.2Ca alloy. The work of Zhou et al. [45] indicated that combined addition of 1.0 wt.% Bi and 0.4 wt.% Sb to AZ91 alloy resulted in more rapid corrosion. In the case of Ge, an early study by McDonald in 1942 [46] investigated a number of Mg binary alloys with Ge alloying additions (0.1~10 wt.%). It was suggested that 0.5~5 wt.% of Ge was the optimum range to improve the yield and tensile strength of the alloys [46]. Recent work by Kim et al. [47] suggested that the corrosion rate of Mg-Ge binary alloys (0.5~2 wt.%) was lower

Mg alloys with heavy alloying loading and Ge alloying can affect the surface film stability [24, 26, 36]. Hanawalt et al. in 1942 [48], suggested that Pb additions did not deteriorate the corrosion of Mg-Pb alloys up to 5 wt.%. The use of Pb alloying to produce Mg anode material has been studied by the works of Wang et al. [49-52] with Mg-6Al-5Pb (wt.%) and Mg-6Al-5Pb-1In (wt.%) alloys; reporting that the Pb containing alloys displayed more significant anodic reaction activity and subsequently demonstrated higher discharging current density output in the context of Mg battery. In another study by Cicek et al., [53] the corrosion resistance of Mg-10Al-12Si alloy (wt.%) was improved with Pb addition (0.2~1 wt.%). Whilst, alloying AZ91 alloy with Pb addition was reported to have a negative effect on the corrosion resistance of the alloy [54]. As similar to Pb, the addition of Sb was also found to be detrimental for the corrosion of AZ91 alloy, which increased cathodic kinetics and led to a more rapid corrosion [54]. As for the case of Sn, Wang et al. [55, 56] indicated that addition of Sn (1~3 wt.%) to Mg-6Al-1Zn and Mg-6Al-5Pb-0.5Mn-0.5RE increased the anodic kinetics of the alloy. Song [57] reported that 2 wt.% of Sn to Mg-7Al-0.2Mn (wt.%) alloy accelerated the anodic kinetics of the alloy. In the binary context, Gu et al. [58] indicated that the corrosion rate of Mg-1Sn (wt.%) was more rapid than pure Mg. Contradictorily, Ha et al. [59] described an extruded Mg-Sn alloy with a heavy Sn loading of 5 wt.%, which displayed improved corrosion resistance in comparison to pure Mg.

The above-mentioned studies generally investigated the corrosion behaviour of Mg alloys with comparatively large alloy loadings of group 14 and 15 alloying elements –with such alloying either utilised as ternary or quaternary alloying additions. In such cases, the impact of the alloying may have been overwhelmed by the complex metallurgical reactions between the alloying additions and other elements (such as Mn and rare earth elements) present. Thus, the primitive influence of group 14 and 15 elements on the corrosion and more specifically, the cathodic reaction kinetics upon Mg, have not been unambiguously elucidated yet. One effort in this aspect has been demonstrated by a recent study by Liu et al., [60] where micro-alloying additions of Ge (0.1 wt.% and 0.3 wt. %) suppressed cathodic kinetics and cathodic activation of Mg, imparting a significant corrosion resistance to Mg.

The work herein was uniquely designed on the basis that the micro additions of group 14 and 15 elements ( $\leq 0.5$  wt.%) were used as a binary alloying addition to Mg, which rules out any possible complex (metallurgical) interactions with other elements in the alloy. The aim of this work is to comprehensively explore the possibility of micro-alloying the elements: Bi, Ge, Pb, Sb and Sn to

ACCEPTED MANUSCRIPT

nominal purity of 99.95 %, from Amac, Australia. Alloying elements including Bi, Ge, Pb, Sb and Sn, were from Alfa-Aesar, USA, acquired with purities of at least 99.9 %. Alloy melting was carried out within a Leybold-Heraeus ISO1/III induction furnace. Prior to melting, induction furnace chamber was evacuated and backfilled with the protective gas consisting of Argon and HFC-134a in a ratio of 10:1; to a positive pressure (of slightly above 1 atm). The alloy melt was heated to 750 °C in a boron nitride coated steel crucible and held for about ~30 mins with at least 4 stirring procedures (using a boron nitride coated steel rod) during this period, to ensure a good mixing. The melt was cast in the protective atmosphere, into a graphite coated steel mould preheated to 200 °C, then left to cool to room temperature.

For each elemental alloying addition studied, two alloys with two target concentrations (in no cases greater than 0.5 wt.%) were produced in this study. The precise chemical composition of the alloys and pure Mg used in this study were independently determined via inductively coupled plasma atomic emission spectroscopy (ICP-AES), by Spectrometer Service (Australia), and the results of which are listed in Table 1.

For all the alloys produced herein, the concentration of impurity elements such as Fe, Cu and Ni, were all well below the so-called impurity threshold value [15, 48], despite the small variation (within 0.01 wt.%). This provides confidence that the findings represent the influence of deliberate alloying elements.

## **2.2 Polarisation experiments**

Specimens for polarisation testing were prepared to a 1200 grit SiC paper finish under ethanol. An electrochemical flat cell (K0235, Princeton Applied Research, USA) was used for all electrochemical tests, employing a 1 cm<sup>2</sup> working electrode, a saturated calomel electrode (SCE) reference electrode and a Pt mesh counter electrode. All electrochemical tests were carried using a Bio-logic VMP 3Z potentiostat.

Unbuffered 0.1 M NaCl (pH 6) was employed as the test electrolyte for all electrochemical testing. In selected tests, to study the effects of pH on the cathodic activation of Mg-alloy specimens, two buffered solutions, 0.1 M NaCl at pH 3 (pH adjusted using 0.1 g/L sodium acetate and 5.9 g/L acetic acid buffer), and 0.1 M NaCl at pH 11 (pH adjusted using 0.9 g/L sodium hydroxide and 2.1

A polarisation scan rate of 1 mV/s was used, with separate anodic and cathodic scans carried out. Anodic scans were carried out from 100 mV below the open circuit potential (OCP) to -1000 mV vs. SCE. Cathodic scans were performed from 20 mV above the OCP to a potential of -2.2 V vs. SCE.

A cyclic galvanostatic-potentiostatic technique was applied for further quantitative analysis of anodically induced cathodic activation of Mg, as used in previous reports focused on testing the cathodic activation of Mg [19, 61, 62]. The technique involved a cyclic anodic galvanostatic current applied in a stepwise increasing manner from 0.025 to 2.5 mA/cm<sup>2</sup> with a 2 min duration for each step. A potentiostatic signal at a fixed potential of -2 V<sub>SCE</sub> was applied in between each anodic polarisation step, in order to evaluate the corresponding cathodic current in response to prior anodic polarisation. The galvanostatic-potentiostatic testing was repeated with a testing regime of higher anodic polarisation current, ranging from 2~24 mA/cm<sup>2</sup> to comprehensively reveal the variation of cathodic current sustained upon Mg surface in response to higher anodic polarisation. The cyclic testing was executed independently in three different electrolytes, using unbuffered 0.1 M NaCl at pH 6 (unbuffered), 0.1 M NaCl at pH 3 (buffered) and 0.1 M NaCl at pH 11 (buffered) to assess the effects of pH on the enhanced cathodic catalytic activity on each anodic polarised Mg alloy specimen surface.

### **2.3 Microstructural analysis**

The microstructure of samples herein was investigated using a JEOL 7001F scanning electron microscope (SEM) in back scattered electron mode (BSE). Specimens for SEM observation were metallographically prepared to 0.05 µm surface finish using colloidal silica suspension. The surface corrosion morphology of specimens after 24 h immersion in 0.1 M NaCl was analysed using an Olympus upright optical microscope.

### **2.4 Mass loss and hydrogen collection**

Mass loss and hydrogen collection testing were carried out to reveal the cumulative corrosion damage on the alloys tested. The preparation and cleaning procedures of immersion test samples were in accordance with the ASTM-G1-03 standard [63]. Specimens for immersion testing were cut from the as-cast ingots and metallographically prepared into cuboids with an exposed surface area of approximately 5 cm<sup>2</sup>. All specimen surfaces were ground to a 1200 grit SiC paper finish and cleaned by sonication in ethanol, followed by accurate measurement and weighing. Immersion testing was performed in quiescent and naturally aerated 0.1 M NaCl at 25 °C for 24 h, during

## 2.5 Atomic emission spectroelectrochemistry (AESEC) measurements

The AESEC measurement as developed by Ogle has been previously described in details [64-67]. This technique involved the use of a scanning flow cell coupled with an inductively coupled plasma optical emission spectrometer (ICP-OES). A flow cell which permits a three-electrode configuration (012799, ALS Co., Ltd, Tokyo, Japan) was used in the studies herein. Unbuffered 0.1 M NaCl was used as the electrolyte, which was continuously pumped through the working electrode surface and onto the ICP-OES instrument using a flow rate of 1.5 mL/s, allowing real time elemental analysis. This method has been shown to have high sensitivity of the detection of dissolved ion concentration, during the process of corrosion or polarisation of Mg [62].

In this study, the concentration of the released  $\text{Mg}^{2+}$  ion was measured as a function of time and related to the instantaneous dissolution rate of Mg samples by equation (1):

$$v_M = C_M \cdot f / A \quad (1)$$

Where  $C_M$  is the volume adjusted ion concentration,  $f$  is the electrolyte flow rate (1.5 mL/s) and  $A$  is the exposed working electrode surface area ( $0.6 \text{ cm}^2$ ). The conversion of the instantaneous dissolution rate to the partial elemental current density ( $j_{\text{Mg}^{2+}}$ ) was determined via Faraday's law, as shown in equation (2):

$$j_M = z \cdot F \cdot v_M \quad (2)$$

Where  $z$  is the valence, equal to 2 for Mg, and  $F$  is the Faraday's constant.

A Bio-logic SP-50 potentiostat was used for the electrochemical control during AESEC. The ICP-OES instrument used in this study was a Perkin Elmer Optima 8000 ICP-OES Spectrometer, which was controlled by Syngistix software. The emission wavelength utilized for Mg was 279.077 nm with a detection limit of  $\sim 1$  ppb.

backscattered electron (BSE) mode using SEM. The general microstructures observed in this work are shown in Fig. 1.

What is evident from Fig. 1 is that the microstructures of pure Mg, Mg-0.5Sn and Mg-0.5Pb alloys were comprised of a single  $\alpha$ -Mg phase; whereas intermetallic phases were observed in the  $\alpha$ -Mg matrix of Mg-0.3Sb, Mg-0.5Bi and Mg-0.3Ge alloys, as evident by particles revealing bright contrast (Fig. 1). The bright contrast revealed by BSE imaging is due to the higher atomic number of the alloying elements (Sb, Bi and Ge) relative to Mg. Such differences in microstructure were expected, owing to the fact that the solid solubility of Sb and Ge, in Mg, is low. It has been reported that the solid solubility of Ge in Mg is about 0.003 at.% at 602 °C and maximum of 0.04 at.% Sb can be dissolved in Mg at 550 °C [68]. Conversely, Bi, Sn and Pb are comparatively more soluble in Mg. The maximum solid solubility of these elements in Mg has been reported to be 1.12 at.%, 3.35 at.% and 7.75 at.% for Bi, Sn and Pb respectively [68]. Mg-0.3Sb alloy had a “rod shape like” and discrete intermetallic phase presented along the grain boundary, which was ascribed to  $Mg_3Sb_2$  (which is also the phase predicted by the Mg-Sb phase diagram). Conversely, extensive eutectic mixtures of “rod shape like” intermetallic phase were seen at the grain boundary of Mg-0.3Ge alloy, which was determined to be  $Mg_2Ge$  (also predicted by the Mg-Ge phase diagram). Mg-0.5Bi alloy appeared to have discrete and spherical shape intermetallic particles dispersed near the “brighter” grain boundary areas, because of the cored solidification microstructure. The intermetallic phase of Mg-0.5Bi was determined to be  $Mg_3Bi_2$  (consistent with the Mg-Bi phase diagram). Given the relative simplicity of the binary Mg alloys, the chemical stoichiometry of intermetallic phases was consistent with the possible phases listed in the relevant equilibrium phase diagrams [68] – and empirically validated by energy dispersive x-ray spectroscopy (EDXS) analysis (which is not shown herein). No alloying segregation from impurity elements, such as Fe, Cu and Ni were observed for all the alloyed specimens and pure Mg studied herein.

### **3.2 Potentiodynamic polarisation response of Mg-alloys**

The typical potentiodynamic polarisation tests were carried out in quintuplicate and the representative polarisation curves of the Mg binary alloys produced herein are given in Fig. 2. Additionally, the curves shown herein include pure Mg (99.95%), representing the benchmark of zero alloying for comparison purposes.

alloying. Most of the alloys tested herein had similar anodic kinetics to that of pure Mg, based on polarisation testing. This is suggestive that these alloying elements have relatively minor effects on the anodic kinetics of Mg. Interestingly, the Mg-0.3Ge and Mg-0.5Pb alloys, however, presented an apparent “passive-type window” on the anodic branch of polarisation curve, ranging from  $E_{\text{corr}}$  to  $\sim 280$  mV above  $E_{\text{corr}}$ . This revelation of a so-called passive-type window was attributed to the negative value of  $E_{\text{corr}}$  which results from the lower cathodic kinetics ( $\sim -1.88$  V<sub>SCE</sub> for Mg-0.3Ge and  $\sim -1.82$  V<sub>SCE</sub> for Mg-0.5Pb) – as previously described for the case of alloying with arsenic [37].

To fully evaluate the effects of alloying on cathodic kinetics, cathodic potentiodynamic polarisation testing with a downward scanning direction from  $E_{\text{corr}}$  to a negative potential ( $-2.2$  V<sub>SCE</sub>), are provided in Fig. 3.

The unique cathodic polarisation curves provide a visual presentation of the impact of the selected alloying elements, indicating a notable shift of cathodic kinetics towards lower rates over a wide range of potentials (Fig. 3). The Mg-0.3Ge and Mg-0.5Pb alloys exhibited the most remarkable decrease in cathodic kinetics. The relative cathodic kinetics among all tested specimens herein, at the potential range between  $E_{\text{corr}}$  and  $-2$  V<sub>SCE</sub>, generally presented in the following order of: Mg-0.5Pb < Mg-0.3Ge < Mg-0.1Sn < Mg-0.3Sb < Mg-0.2Sb < Mg-0.1Bi < Mg-0.1Pb < Mg-0.1Ge < Mg-0.5Bi < Mg-0.5Sn < Mg.

### **3.3 Mass loss and hydrogen collection of Mg-alloys.**

Potentiodynamic polarisation provides an instantaneous and quantitative analysis of the relative anodic and cathodic kinetics for the alloys; whereas it is not the most effective measurement for the determination of long term corrosion performance. The long-term testing at open circuit potential (OCP) is indeed an important method to rationalise the longer term corrosion behaviour. King et al.[69] reported a combined corrosion measurement, which includes electrochemical impedance spectroscopy (EIS), mass loss and hydrogen collection for the accurate determination of Mg corrosion. This technique was also validated in other independent studies of corrosion of Mg and its alloys [70, 71]. The study herein adopted the simultaneous measurement of mass loss and hydrogen collection (in the absence of EIS, which remains an important aspect of future work) over a 24 h duration in 0.1 M NaCl (unbuffered, pH 6). The pH of the solution increased to  $\sim 10$  after the

significant decrease in the corrosion rate of the Mg alloys containing group 14 and 15 elements in comparison to that of pure Mg. The extent of reduction of corrosion rate by alloying was about one order magnitude, on the basis of measured mass loss (Fig. 4a) and hydrogen gas evolved (Fig. 4b). Of all the tested Mg binary alloys herein, Mg-0.3Ge and Mg-Pb (with 0.1 and 0.5 wt.% alloying additions) alloys exhibited the largest improvement in corrosion resistance. It was also noted that other Mg alloys tested herein also revealed distinct corrosion performance, the merits of which, however, were not clearly indicated by prior polarisation testing. The primary reason for this is likely due to the fact that the cathodic activation and corrosion of Mg are time-dependent processes [21, 39] and the suppression of cathodic kinetics by alloying might become more predominant during the dissolution process of Mg. In addition, it was determined that corrosion rate of Mg alloys tested herein did not change linearly with the corresponding alloy loading (alloying element concentration). For instance, the rate of mass loss and hydrogen evolution for Mg-0.5Sn was ~5 times higher than that of Mg-0.1Sn; whilst, the corrosion rate of Mg-0.3Ge was approximately ~3 times lower in comparison to that of Mg-0.1Ge.

### **3.4 Corrosion morphology following 24h of exposure in 0.1 M NaCl**

Optical micrographs of the surface morphology for the specimens tested herein, before and after the immersion / exposure testing (0.1 M NaCl for 24 h) are shown in Fig. 5.

It was observed that a wide spread dark “filiform-like” corrosion morphology was present on the surface of pure Mg. This filiform-like corrosion morphology has been previously noted as typical for pure Mg and many Mg alloys [3, 19, 62, 72, 73], and is of relevance to the evolution of local cathodes and anodes, during the corrosion process of Mg [20-22].

In contrast, the corrosion morphology of the binary Mg-alloys revealed a comparatively minor extent of corrosion attack, concomitant with discrete corrosion sites. Such a distinct change in the corrosion morphology reveals the ability of group 14 and 15 alloying elements to inhibit the typical “filiform like” corrosion. The formation of this type of dark “filiform like” film is suggestive of enhanced cathodic activity upon corroded Mg surface [20, 39, 62]. As such, the differing corrosion morphology of the Mg binary alloys is posited to be related to the ability of the group 14 and 15 element additions to hinder the propagation of dark filiform-like corrosion films and to suppress cathodic activation.

anodically polarised via stepwise galvanostatic cycles; whilst a cathodic potentiostatic signal at the fixed potential of  $-2 V_{SCE}$  was applied between each anodic polarisation step to assess the cathodic kinetics in response to prior anodic polarisation. The abridged results of the galvanostatic-potentiostatic experiments for the binary Mg-alloys containing group 14 and 15 elements and pure Mg are seen in Fig. 6.

Fig. 6a reveals the data collected for the alloys tested under the anodic polarisation cycles from 0.025 to 2.5 mA/cm<sup>2</sup>. What can be readily observed is that measured cathodic current density increased after each anodic polarisation step for pure Mg. This indicates that enhanced cathodic kinetics of Mg arose from the prior anodic polarisation, which is also consistent with the previously reported works regarding the electrochemical evidence of anodically induced cathodic activation [19, 61].

In the case of the Mg binary alloys studied, a marked decrease in the cathodic current density is observed (Fig. 6a); for example Mg-0.3Ge and Mg-0.3Sb alloys revealed a sustained lower cathodic current density by about a one order magnitude in contrast to (pure) Mg. Another salient feature seen from Fig. 6a is that the recorded cathodic current density of the Mg alloys remained essentially constant, irrespective of prior anodic polarisation. Such a stabilised cathodic current density following prior cyclic anodic polarisation suggests the ability of alloying additions of Bi, Ge, Pb, Sb and Sn to halt the cathodic activation of Mg.

The cyclic galvanostatic-potentiostatic experiment was further carried out with a higher anodic dissolution range from 2 to 24 mA/cm<sup>2</sup>, as seen in Fig. 6b. A similar trend was observed for pure Mg, which displayed evidence of cathodic activation after polarisation. The binary Mg-alloys presented a lower cathodic current density in comparison to that of pure Mg, however a slight enhancement of cathodic kinetics was observed for the binary Mg-alloys when the applied dissolution current density was larger than 10 mA/cm<sup>2</sup>. It is noted however, that 10 mA/cm<sup>2</sup> is an exceptionally high current density that is concomitant with extensive dissolution – and hence an extreme test [39, 74].

The pH of the test electrolyte (which was originally pH 6) increased to ~9 after the 0.025 to 2.5 mA/cm<sup>2</sup> cyclic galvanostatic-potentiostatic experiment, whilst the pH of the test electrolyte increased to ~10 following the experiment with 2 to 24 mA/cm<sup>2</sup> dissolution range. It merits

In order to comprehensively assess the variation of cathodic kinetics in response to a prior anodic polarisation cycle of varying pH, cyclic testing with two exposure regimes (both 0.025~2.5 mA/cm<sup>2</sup> and 2~24 mA/cm<sup>2</sup>) was repeated in isolated experiments using buffered 0.1 M NaCl at two different pH values of 3 and 11.

The abridged results of the cyclic testing with the exposure regimes in 0.1 M NaCl at pH 3 for alloyed specimens and pure Mg are shown in Fig. 7; where it was seen that cathodic current density measured upon pure Mg increased slightly, following an increase in the prior anodic dissolution current density. What is noted from the response of the binary Mg alloys is that the measured cathodic current density remained relatively constant, in spite of the aggressive nature of the test (which is also concomitant with surface area alteration induced by the high rates of dissolution in acidic solution). The empirical testing reveals that there was no appreciable enhancement of cathodic kinetics upon anodically polarised Mg surfaces in 0.1 M NaCl buffered at pH 3. However, it is noteworthy that a lower cathodic current density (relative to pure Mg) was also realised in Mg-binary alloys with addition of 0.1 wt.% Pb, 0.5 wt.% Pb and 0.2 wt.% Sb.

Figure 8 reveals the superimposed results of cyclic galvanostatic-potentiostatic testing in 0.1 M NaCl at pH 11. A well-pronounced enhancement of cathodic kinetic for pure Mg was observed, indicative of significant cathodic activation in alkaline solution. The cathodic kinetics of the binary Mg alloys remained relatively steady in response to anodic polarisation in the range of 0.025~2.5 mA/cm<sup>2</sup> (Fig. 8a), whilst only a slight enhancement was observed when tested after exposure to the greater anodic range of 2~24 mA/cm<sup>2</sup> (Fig. 8b). It may also be seen from Fig. 8 that the magnitude of cathodic current density sustained upon the Mg alloys with 0.3 wt.% Ge and 0.5 wt.% Pb was about one order magnitude lower than pure Mg over the range of all prior anodic polarisation conditions.

Overall, the results from galvanostatic-potentiostatic experiments in 0.1 M NaCl of varying pH (Fig. 6-8), reveal the relative extent of cathodic activation for the alloys investigated herein. It was determined that the cathodic (HER) kinetics sustained by the specimens studied were lower in acidic conditions and higher in alkaline conditions. The incremental increase of cathodic activation was proportional to the increasing pH of the electrolyte. For example, the value of the cathodic current density sustained upon Mg following the cyclic anodic polarisation regime (0.025 to 2.5 mA/cm<sup>2</sup>) was about ~1.67 times of the pre-anodic polarisation value at unbuffered pH 6; whilst the

cathodic activation of Mg in an aqueous environment over a wide pH range.

### 3.6 AESEC analysis of Mg-alloys

The at open circuit potential (OCP) Mg dissolution current density ( $j_{\text{Mg}^{2+}}$ ) of the binary Mg alloys with group 14 and 15 additions was determined from the concentration of  $\text{Mg}^{2+}$  measured by ICP-OES of downstream electrolyte (Fig. 9). Additionally, the data collected for pure Mg is also included in the plots for comparison purpose.

What is observed from inspection of Fig. 9 is that, for most Mg alloys, a peak of  $j_{\text{Mg}^{2+}}$  commenced immediately upon the initial few seconds' exposure to 0.1 M NaCl. Following this peak of early dissolution,  $j_{\text{Mg}^{2+}}$  gradually decreased to a plateau current density. The attainment of the relatively steady dissolution current density at OCP is ascribed to the formation of the surface film, which developed rapidly upon exposure to an electrolyte. Whilst, the exceptional case is the Mg-0.3Ge alloy, where a relatively constant and lower value of  $j_{\text{Mg}^{2+}}$  at OCP is observed, indicating a steady dissolution rate of the alloy.

From Fig. 9, it can be seen that pure Mg sustained the highest dissolution current density at OCP, being in the range of  $\sim 150$  to  $\sim 120 \mu\text{A}/\text{cm}^2$ . This suggests that Mg corroded readily in the absence of any external polarisation. In contrast, the dissolution rate of the Mg alloys was much lower than that of Mg at OCP, whilst the minimum dissolution rate measured was  $\sim 70 \mu\text{A}/\text{cm}^2$  with Mg-0.3Ge alloy. The relatively constant and lower value of  $j_{\text{Mg}^{2+}}$  sustained upon Mg-0.3Ge alloy reveals that alloying affects the partial anodic reactions at the condition of free corrosion (recalling that ICP-OES can only determine the rate of the anodic reaction). Polarisation testing in 0.1 M NaCl was carried out after 10 min OCP exposure to 0.1 M NaCl, using an electrochemical flow cell coupled to ICP-OES. The representation of polarisation data for the Mg alloys produced herein, along with the comparison of pure Mg is shown in Fig. 10.

Figure 10a presents the AESEC determined dissolution current density as a function of polarisation time (the term AESEC used to describe the online ICP-OES analysis in the presence of an external polarisation). The polarisation test was commenced from 100 mV below OCP to  $-1 V_{\text{SCE}}$  with a potential scan rate of 1 mV/s. Thus, in the initial 100s, the specimens were cathodically polarised. The dissolution current density of all the Mg alloys including pure Mg was slightly decreased within  $\sim 5 \mu\text{A}/\text{cm}^2$  range during cathodic polarisation until  $E_{\text{corr}}$  was reached. This indicates a

66, 77, 78]. Upon the transition to anodic polarisation, the dissolution current density of the Mg alloys increased with increasing applied anodic potential. It can be seen that at the maximum anodic potential ( $-1 V_{SCE}$ ), dissolution current density sustained upon pure Mg was  $\sim 140 \mu A/cm^2$ . In contrast, the dissolution current density of the alloyed specimens with the maximum anodic polarisation was in the range of  $\sim 80$  to  $\sim 100 \mu A/cm^2$ , revealing a lower corrosion rate of the alloys associated that is also related to a reduction of the anodic partial current density independent of any other effects such as those on the cathodic partial current density. Again, it is emphasised for the purposes of interpretation, that AESEC analysis only probes the anodic partial reaction.

To further supplement the data in Fig. 10a, polarisation data presented in the format of applied potential versus log dissolution current density determined from AESEC analysis, as seen in Fig. 10b. It may be observed from Fig. 10b that the dissolution rate of pure Mg was comparatively higher than that of the custom prepared binary Mg alloys throughout the whole range of potentials applied. For potentials  $< \sim -1.6 V_{SCE}$ , the alloys displayed the trend of an initial slight decrease in  $j_{Mg^{2+}}$  under cathodic polarisation and subsequent  $j_{Mg^{2+}}$  fluctuation upon polarisation to  $E_{corr}$ . In the case of anodic polarisation ( $> \sim -1.6 V_{SCE}$ ),  $j_{Mg^{2+}}$  increased log-linearly with the applied potential, which represents “Tafel-type behaviour”. The Tafel slope of the binary alloys produced herein is higher than that of pure Mg. This further reveals the functionality of the group 14 and 15 alloying elements to suppress the dissolution of Mg while potentiodynamically polarised, independent of cathodic processes; a notion not previously reported. The polarisation curves obtained during AESEC analysis (Fig. 10b) exhibit a substantial decrease in anodic partial current density both at OCP and under polarisation for all the binary Mg alloys in contrast to pure Mg. Such a feature was not readily revealed by polarisation experiments directly measured from the potentiostat with a conventional electrochemical cell (Fig. 2), whereby the alloyed specimens exhibited similar anodic kinetics. In conventional electrochemical testing, the measured currents are a summation of anodic and cathodic reaction rates, however, AESEC is able to decouple the anodic reaction rate uniquely.

The primary reactions involved under anodic polarisation of Mg can be described by reactions (3) - (6) [3].



dissolution process of Mg. The reaction (5) occurs due to the localised alkalisation, as previously mentioned; whilst the reaction (6) is the overall reaction of reaction (3)-(5). The anodic and cathodic current densities are defined as  $j_a$  and  $j_c$  respectively. The net current density measured by the potentiostat,  $j_{net}$  under anodic polarisation can be defined by the equation (7):

$$j_{net} = j_a - j_c \quad (7)$$

According to the Butler-Volmer equation, the cathodic reaction rate,  $j_c$  should decrease with the increasing potential [13]. Whereas cathodic activation of Mg occurred under anodic polarisation, the  $j_c$  continued to increase with the increase of applied potential. In many cases, some electrons generated by localised cathodic reactions or the direct formation of  $Mg(OH)_2$  by reaction (6) were not fully tallied by the potentiostat. Thus, the value of net current density  $j_{net}$  underestimates the dissolution rate of Mg samples, owing to the anodic polarisation induced cathodic activation. However, the alloying applied herein suppressed the cathodic kinetics and cathodic activation of Mg, which (in some cases significantly) reduced the value of  $j_c$  and suppressed cathodic activation; resulting in a similar  $j_{net}$  value for all the alloys. In contrast, the value of  $j_{Mg^{2+}}$  determined by AESEC analysis was independent of the alteration of cathodic current density during anodic polarisation. Furthermore, the lower magnitude of ICP determined dissolution current density (in comparison to that measured by potentiostat) suggests that a large fraction of ionised Mg species were involved in the formation of an insoluble film upon the surface of Mg (shown by reaction (6)) as a result of dissolution [35, 62].

### 3.7 General discussion

Micro-alloying additions of group 14 and 15 elements to Mg notably decreased cathodic kinetics and were associated with a significant improvement of corrosion resistance for the binary Mg alloys produced herein. This was further interpreted by the lower value of mass loss and hydrogen evolved, following 24 h immersion in 0.1 M NaCl. The functionality of the alloying also includes a drastically-changed corrosion morphology from typical wide-spread “filiform-like” corrosion to superficial “discrete corrosion sites”.

The potentiodynamic polarisation results conventionally measured with a potentiostat and static electrochemical cell indicated similar anodic kinetics for the binary Mg-alloys and pure Mg, which

produced herein was lower than that of pure Mg at OCP and during polarised conditions.

The alloying additions of group 14 and 15 elements: Bi, Ge, Pb, Sb and Sn were determined to achieve similar cathodic poisoning effects on the corrosion of Mg, as previously reported in the Mg-As alloy [37]. Of all the alloys tested, Mg-0.3Ge alloy was demonstrated to possess the lowest cathodic reaction kinetics and the highest corrosion resistance.

The detailed mechanism of cathodic activation has yet to be determined. It has been hypothesised that impurity metals such as Fe, or Fe rich second phases, which have a low solid solubility and high over-potential for HER, could serve as primary cathodic sites that sustain the cathodic activity upon dissolving Mg [15, 40, 79]. A so called threshold value of impurity tolerance limit has also been defined (~170 ppm for Fe), beyond which the corrosion rate of Mg will significantly increase [2, 15, 80, 81]. The enrichment of the noble metal impurities following dissolution at OCP or anodic polarisation was expected to enhance the cathodic activity, because of the increase of the net area of the cathodic sites [19, 20, 82-84]. The presence of the noble metal impurity enrichment has also been validated by several independent studies, which employed a combination of methodologies including high resolution microscopy [84, 85], Rutherford Backscatter Spectroscopy (RBS) [86] as well as nuclear microprobe particle induced X-ray emission (PIXE) analysis [83]. Therefore, it is assumed that the enrichment of Fe containing phase could be associated with the cathodic activation of Mg. It has also been known in other fields that the kinetics of HER upon Fe has been dramatically affected by the presence of electro-catalytic poisons such as arsenic, antimony, bismuth and tin [40, 41, 87-91]. The adsorption of the cathodic poisons upon electrode surface reduced the surface coverage of hydrogen atom intermediate and restricted the recombination absorbed hydrogen atom intermediate, thus retarding the rate of HER [88, 90, 92-94]. It is, therefore, reasonably hypothesised that, the alloying elements used in this work might achieve similar poisoning effect in Mg, whereby deactivated the enriched Fe or Fe containing phase towards HER and suppressed cathodic activation.

Nevertheless, Lysne, et al., proposed a model to estimate the Fe enrichment following anodic polarisation based on Mg samples containing a different range of Fe concentration (ranging from 25 ppmw to 13000 ppmw) [95]. It was revealed that the efficiency of Fe enrichment following anodic dissolution was estimated to be low (less than 1%). In addition, the enhanced cathodic activity was

Cyclic electrochemical experiments in electrolytes of varying pH were performed as a complementary test to further assess the cathodic activation tendency of the Mg binary alloys. The results demonstrated the ability of the alloying to suppress cathodic activation produced by prior anodic dissolution cycles in a wide range of pH. Such results provide a meaningful approach for utilising Mg alloys as electrode materials for example, in Mg primary batteries. Hydrogen evolution and “parasitic discharge” issues that occur during the on-off cycles for Mg primary batteries, often are associated to premature battery failure [9, 10].

The extent of cathodic activation upon Mg specimens was also observed to increase with increasing electrolyte pH. As per thermodynamics (also visually revealed by the Pourbaix diagram [12]), Mg has a higher tendency for the formation of magnesium hydroxide ( $\text{Mg}(\text{OH})_2$ ) in more alkaline solution, or in the vicinity of the Mg surface where HER occurs. Thus, there is significance between the presence of hydroxide films and the manifestation of cathodic activation for Mg. Such notion is in accordance with other contemporary studies of Mg dissolution including first principles modelling [61, 72, 78, 97-99]. The role of the group 14 and 15 elements studied herein with respect to the development of surface hydroxide films was not investigated in the present work, but remains important future work.

It is noted that only a dilute concentration of alloying (in all cases no larger than 0.5 wt.%) was deliberately added into Mg in this work. The micro-alloying additions of the elements that are relatively soluble in Mg (Pb and Sn) resulted in minor microstructure alteration of Mg and most of the alloying were present in the solid solution of Mg. Conversely, elements with lower solid solubility (Bi, Ge and Sb) influenced the microstructure by stimulating second phase particles in addition to alloying the solid solution of Mg. A recent study using density functional theory (DFT) calculations investigated the influence of dilute alloy loadings (~1 at.%) of a wide range of alloying elements upon a Mg slab model with (0001) orientation towards HER [100]. The DFT calculations suggested that the elements including Ge, Sb and Sn made the HER less thermodynamically favourable on Mg surface by the means of destabilising the water dissociation reaction and repelling the adsorbed hydrogen atoms [100]. It may be reasonably assumed that alloying with group 14 and 15 elements substituted in the solid solution of Mg (akin to the dilute alloyed Mg slab model in the DFT calculation) may also play an important role in suppressing the cathodic activity, in addition to the possible “poisoning effects” on any Fe containing phases. The partial anodic

Mg alloys. Furthermore, it is also of great relevance for the development of corrosion resistant Mg electrode materials and self-discharge resistant Mg primary batteries. The use of the group 14 and 15 elements as ternary or quaternary combinations for Mg alloys production should also be investigated in future, aiming to produce Mg alloys with both appreciable corrosion resistance and desirable mechanical properties.

ACCEPTED MANUSCRIPT

1. Microalloying additions of Ge, Sb, Pb, Sn and Bi demonstrated a marked ability in decreasing cathodic kinetics upon Mg, in the order they were listed.
2. In addition to the suppression of cathodic kinetics, alloying additions explored herein also imparted appreciable corrosion resistance to Mg, as evident from the mass loss experiment, hydrogen collection and AESEC testing. Of all the composition tested, 0.3 wt.% Ge was empirically determined – from the compositions studied herein - to be the most effective alloying addition in the context of corrosion control.
3. The corrosion morphology of Mg following 24 h exposure in 0.1 M NaCl was significantly altered from the typical extensive filiform-like corrosion attack to less extensive and discrete corrosion sites; influenced by alloying. The changes of corrosion morphologies are posited to be associated with the ability of specific alloying additions to stifle cathodic activation – and hence the form of corrosion propagation upon Mg.
4. The custom produced binary Mg-alloys remain more resistant to cathodic activation in comparison to pure Mg, over a wide range of pH, as revealed by the cyclic potentiostatic-galvanostatic testing carried out in 0.1 M NaCl of varying pH. This result provides an attractive outcome in the context of applying Mg-based electrodes as the more reliable electrode materials in primary battery systems.
5. The AESEC experiment herein, capable of detecting dissolved  $\text{Mg}^{2+}$  arising from Mg corrosion or anodic dissolution, reveals the ability of alloying elements explored herein to hinder the corrosion of Mg. It was demonstrated that the partial anodic kinetics of the alloys was lower than that of pure Mg, at OCP and during polarised conditions. This is an important finding and not been previously revealed, as studies of Mg alloys using AESEC are to date scarce. Additionally, AESEC analysis revealed that the dissolution of Mg is not suppressed at low cathodic over-potentials, up to 100 mV below OCP. The difference between currents measured from conventional potentiodynamic polarisation and the  $j_{\text{Mg}^{2+}}$  measured from AESEC is suggestive that a fraction of dissolved  $\text{Mg}^{2+}$  is involved in the formation of subsequently insoluble films upon the Mg surfaces, concomitant with other studies.

ACCEPTED MANUSCRIPT

- [4] M. Easton, M. Gibson, A. Beer, M. Barnett, C. Davies, T. Durandet, S. Blacket, X. Chen, N. Birbilis, T. Abbott, The Application of Magnesium Alloys to the Lightweighting of Automotive Structures, in: A. Subic, J. Wellnitz, M. Leary, L. Koopmans (Eds.) Sustainable Automotive Technologies 2012, Springer Berlin Heidelberg, 2012, pp. 17-23.
- [5] T. Abbott, Corrosion, 71 (2015) 120-127.
- [6] L. Yin, X. Huang, H. Xu, Y. Zhang, J. Lam, J. Cheng, J.A. Rogers, Advanced materials, 26 (2014) 3879-3884.
- [7] V. Edupuganti, R. Solanki, Journal of Power Sources, 336 (2016) 447-454.
- [8] M. Esmaily, J.E. Svensson, S. Fajardo, N. Birbilis, G.S. Frankel, S. Virtanen, R. Arrabal, S. Thomas, L.G. Johansson, Progress in Materials Science, 89 (2017) 92-193.
- [9] P. Saha, M.K. Datta, O.I. Velikokhatnyi, A. Manivannan, D. Alman, P.N. Kumta, Progress in Materials Science, 66 (2014) 1-86.
- [10] L.D. Chen, J.K. Nørskov, A.C. Luntz, The Journal of Physical Chemistry C, 119 (2015) 19660-19667.
- [11] N. Wang, R. Wang, Y. Feng, W. Xiong, J. Zhang, M. Deng, Corrosion Science, (2016).
- [12] M. Pourbaix, Atlas of electrochemical equilibria in aqueous solutions, 2nd English ed., National Association of Corrosion Engineers, Houston, Tex., 1974.
- [13] D.A. Jones, Principles and prevention of corrosion, 2nd ed., Prentice Hall, Upper Saddle River, NJ, 1996.
- [14] W. Beetz, Philosophical Magazine Series 32 (1866) 269-278.
- [15] R.E. McNulty, J.D. Hanawalt, Transactions of The Electrochemical Society, 81 (1942) 423-433.
- [16] J.L. Robinson, P.F. King, Journal of The Electrochemical Society, 108 (1961) 36-41.
- [17] N.T. Kirkland, G. Williams, N. Birbilis, Corrosion Science, 65 (2012) 5-9.
- [18] G.S. Frankel, A. Samaniego, N. Birbilis, Corrosion Science, 70 (2013) 104-111.
- [19] N. Birbilis, A.D. King, S. Thomas, G.S. Frankel, J.R. Scully, Electrochimica Acta, 132 (2014) 277-283.
- [20] G. Williams, N. Birbilis, H.N. McMurray, Electrochemistry Communications, 36 (2013) 1-5.
- [21] G. Williams, N. Birbilis, H.N. McMurray, Faraday discussions, 180 (2015) 313-330.
- [22] G. Williams, H.N. McMurray, Journal of the Electrochemical Society, 155 (2008) C340.
- [23] X.B. Chen, N. Birbilis, T.B. Abbott, Corrosion, 67 (2011) 035005-035001-035005-035016.
- [24] K. Gusieva, C.H.J. Davies, J.R. Scully, N. Birbilis, International Materials Reviews, 60 (2015) 169-194.
- [25] Y.J. Wu, X.B. Chen, G. Williams, J.R. Scully, T. Gengenbach, N. Birbilis, RSC Adv., 6 (2016) 43408-43417.
- [26] X. Xia, C.H.J. Davies, J.F. Nie, N. Birbilis, Corrosion, 71 (2015) 38-49.
- [27] J.F. Nie, Physical Metallurgy of Light Alloys, in: D.E.L. Hono (Ed.) Physical Metallurgy (Fifth Edition), Elsevier, Oxford, 2014, pp. 2009-2156.
- [28] Y. Zhang, T. Alam, B. Gwalani, W. Rong, R. Banerjee, L.-M. Peng, J. Nie, N. Birbilis, Philosophical Magazine Letters, 96 (2016) 212-219.
- [29] N. Birbilis, M.A. Easton, A.D. Sudholz, S.M. Zhu, M.A. Gibson, Corrosion Science, 51 (2009) 683-689.
- [30] A.D. Südholz, K. Gusieva, X.B. Chen, B.C. Muddle, M.A. Gibson, N. Birbilis, Corrosion Science, 53 (2011) 2277-2282.
- [31] D.S. Gandel, M.A. Easton, M.A. Gibson, T. Abbott, N. Birbilis, Corrosion Science, 81 (2014) 27-35.
- [32] J.O.M. Bockris, A.K.N. Reddy, Modern Electrochemistry 2B, Springer US, Boston, 2007.

- The Electrochemical Society, 165 (2016) C324-C329.
- [36] A. Samaniego, K. Gusieva, I. Llorente, S. Feliu, N. Birbilis, *Corrosion Science*, 89 (2014) 101-110.
- [37] N. Birbilis, G. Williams, K. Gusieva, A. Samaniego, M.A. Gibson, H.N. McMurray, *Electrochemistry Communications*, 34 (2013) 295-298.
- [38] D. Eaves, G. Williams, H.N. McMurray, *Electrochimica Acta*, 79 (2012) 1-7.
- [39] G. Williams, H.A.-L. Dafydd, H.N. McMurray, N. Birbilis, *Electrochimica Acta*, 219 (2016) 401-411.
- [40] J.O.M. Bockris, B.E. Conway, *Transactions of the Faraday Society*, 45 (1949) 989-999.
- [41] P. Stonehart, G. Kohlmayr, *Electrochimica Acta*, 17 (1972) 369-382.
- [42] A.J. Bard, J.A.A. Ketelaar, *Journal of The Electrochemical Society*, 121 (1974) 212C.
- [43] H. Wendt, E.V. Spinacé, A. Oliveira Neto, M. Linardi, *Química Nova*, 28 (2005) 1066-1075.
- [44] H.Y. Tok, E. Hamzah, H.R. Bakhsheshi-Rad, *Journal of Alloys and Compounds*, 640 (2015) 335-346.
- [45] W. Zhou, N.N. Aung, Y. Sun, *Corrosion Science*, 51 (2009) 403-408.
- [46] J. McDonald, *Magnesium Base Alloy*, in, Dow Chemical Co, 1942.
- [47] B. Kim, K. Park, H. Kimura, Y. Park, I. Park, *Materials Transactions*, 53 (2012) 240-243.
- [48] J.D. Hanawalt, C.E. Nelson, J.A. Peloubet, *Trans AIME*, (1942).
- [49] N. Wang, R. Wang, C. Peng, Y. Feng, X. Zhang, *Transactions of Nonferrous Metals Society of China*, 20 (2010) 1403-1411.
- [50] N. Wang, R. Wang, C. Peng, Y. Feng, X. Zhang, *Transactions of Nonferrous Metals Society of China*, 20 (2010) 1936-1943.
- [51] N. Wang, R. Wang, C. Peng, Y. Feng, B. Chen, *Corrosion Science*, 64 (2012) 17-27.
- [52] N. Wang, R. Wang, C. Peng, B. Peng, Y. Feng, C. Hu, *Electrochimica Acta*, 149 (2014) 193-205.
- [53] B. Çiçek, Y. Sun, *Materials & Design*, 37 (2012) 369-372.
- [54] A.D. Südholz, N. Birbilis, C.J. Bettles, M.A. Gibson, *Journal of Alloys and Compounds*, 471 (2009) 109-115.
- [55] P. Wang, J. Li, Y. Guo, Z. Yang, F. Xia, J. Wang, *Rare Metals*, 30 (2011) 639-643.
- [56] P. Wang, J. Li, Y. Guo, Z. Yang, F. Xia, J. Wang, *Rare Metal Materials and Engineering*, 41 (2012) 2095-2099.
- [57] G.-L. Song, *Corrosion Science*, 51 (2009) 2063-2070.
- [58] X. Gu, Y. Zheng, Y. Cheng, S. Zhong, T. Xi, *Biomaterials*, 30 (2009) 484-498.
- [59] H.-Y. Ha, J.-Y. Kang, J. Yang, C.D. Yim, B.S. You, *Corrosion Science*, 102 (2016) 355-362.
- [60] R.L. Liu, M.F. Hurley, A. Kvryan, G. Williams, J.R. Scully, N. Birbilis, *Scientific reports*, 6 (2016) 28747.
- [61] R.L. Liu, S. Thomas, J.R. Scully, G. Williams, N. Birbilis, *Corrosion*, (2017) 469-505.
- [62] S. Thomas, O. Gharbi, S.H. Salleh, P. Volovitch, K. Ogle, N. Birbilis, *Electrochimica Acta*, 210 (2016) 271-284.
- [63] A. International, *ASTM Standard G1-03*, in: *Standard Practice for Preparing, Cleaning, and Evaluating Corrosion Test Specimens*, PA: ASTM International, West Conshohocken, 2011.
- [64] S. Lebouil, O. Gharbi, P. Volovitch, K. Ogle, *Corrosion*, 71 (2015) 234-241.
- [65] S. Lebouil, A. Duboin, F. Monti, P. Tabeling, P. Volovitch, K. Ogle, *Electrochimica Acta*, 124 (2014) 176-182.
- [66] J. Światowska, P. Volovitch, K. Ogle, *Corrosion Science*, 52 (2010) 2372-2378.
- [67] K. Ogle, *Corros. Mater.*, 37 (2012) 58-65.

- (2015) C403-C411.
- [72] S.H. Salleh, S. Thomas, J.A. Yuwono, K. Venkatesan, N. Birbilis, *Electrochimica Acta*, 161 (2015) 144-152.
- [73] S. Li, A.C. Bacco, N. Birbilis, H. Cong, *Corrosion Science*, 112 (2016) 596-610.
- [74] S. Fajardo, C.F. Glover, G. Williams, G.S. Frankel, *Electrochimica Acta*, 212 (2016) 510-521.
- [75] K.D. Ralston, G. Williams, N. Birbilis, *Corrosion*, 68 (2012).
- [76] L. Rossrucker, A. Samaniego, J.P. Grote, A.M. Mingers, C.A. Laska, N. Birbilis, G.S. Frankel, K.J.J. Mayrhofer, *Journal of the Electrochemical Society*, 162 (2015) C333-C339.
- [77] L. Rossrucker, K.J.J. Mayrhofer, G.S. Frankel, N. Birbilis, *Journal of the Electrochemical Society*, 161 (2014) C115-C119.
- [78] T.W. Cain, M.A. Melia, J.M. Fitz-Gerald, J.R. Scully, *Corrosion*, 73 (2017) 544-562.
- [79] R. Glicksmann, *Journal of the Electrochemical Society*, 106 (1959) 83.
- [80] M. Liu, G.-L. Song, *Corrosion Science*, 77 (2013) 143-150.
- [81] S. Simanjuntak, M.K. Cavanaugh, D.S. Gandel, M.A. Easton, M.A. Gibson, N. Birbilis, *Corrosion*, 71 (2014) 199-208.
- [82] D. Hoche, C. Blawert, S.V. Lamaka, N. Scharnagl, C. Mendis, M.L. Zheludkevich, *Physical chemistry chemical physics : PCCP*, 18 (2016) 1279-1291.
- [83] N. Birbilis, T. Cain, J.S. Laird, X. Xia, J.R. Scully, A.E. Hughes, *ECS Electrochemistry Letters*, 4 (2015) C34-C37.
- [84] M. Taheri, J.R. Kish, N. Birbilis, M. Danaie, E.A. McNally, J.R. McDermid, *Electrochimica Acta*, 116 (2014) 396-403.
- [85] M. Taheri, R.C. Phillips, J.R. Kish, G.A. Botton, *Corrosion Science*, 59 (2012) 222-228.
- [86] T. Cain, S.B. Madden, N. Birbilis, J.R. Scully, *Journal of the Electrochemical Society*, 162 (2015) C228-C237.
- [87] M. Smialowski, *Hydrogen in steel : effect of hydrogen on iron and steel during production, fabrication and use*, Oxford : Pergamon ; Warsaw : Wydawnictwa Naukowe -Techniczne 1962.
- [88] B.E. Conway, B.V. Tilak, 38 (1992) 1-147.
- [89] L.J. Gao, S.Y. Qian, B.E. Conway, *Journal of Applied Electrochemistry*, 26 (1996) 803-814.
- [90] S.Y. Qian, B.E. Conway, G. Jerkiewicz, *Journal of the Chemical Society, Faraday Transactions*, 94 (1998) 2945-2954.
- [91] R. Winston, *Oil and Gas Pipelines: Integrity and Safety Handbook*, Hoboken, New Jersey : Wiley 2015.
- [92] E.G. Dafft, K. Bohnenkamp, H.J. Engell, *Chemischer Informationsdienst*, 10 (1979).
- [93] B.E. Conway, G. Jerkiewicz, *Journal of Electroanalytical Chemistry*, 357 (1993) 47-66.
- [94] J.M. Jaksic, N.M. Ristic, N.V. Krstajic, M.M. Jaksic, *International Journal of Hydrogen Energy*, 23 (1998) 1121-1156.
- [95] D. Lysne, S. Thomas, M.F. Hurley, N. Birbilis, *Journal of the Electrochemical Society*, 162 (2015) C396-C402.
- [96] S. Fajardo, G.S. Frankel, *Electrochimica Acta*, 165 (2015) 255-267.
- [97] T.W. Cain, I. Gonzalez-Afanador, N. Birbilis, J.R. Scully, *Journal of The Electrochemical Society*, 164 (2017) C300-C311.
- [98] J.A. Yuwono, N. Birbilis, K.S. Williams, N.V. Medhekar, *The Journal of Physical Chemistry C*, (2016).
- [99] K.S. Williams, V. Rodriguez-Santiago, J.W. Andzelm, *Electrochimica Acta*, 210 (2016) 261-270.
- [100] K.R. Limmer, K.S. Williams, J.P. Labukas, J.W. Andzelm, *Corrosion*, 73 (2017) 506-517.

**Table 1.** Composition (in wt. %) of samples tested herein. Compositions were independently analysed.

Sample	Mg	Al	Zn	Cu	Si	Fe	Ca	Mn	Ni	Sb	Pb
<b>Mg</b>	Bal.	0.005	0.005	0.002	0.02	0.006	0.001	0.01	0.001	-	-
<b>Mg-0.2Sb</b>	Bal.	0.005	0.004	0.001	0.03	0.002	0.003	0.01	0.001	0.23	-
<b>Mg-0.3Sb</b>	Bal.	0.01	0.01	0.001	0.02	0.001	0.01	0.03	0.001	0.32	-
<b>Mg-0.1Bi</b>	Bal.	0.01	0.01	0.001	0.01	0.001	0.01	0.03	0.001	-	0.01
<b>Mg-0.5Bi</b>	Bal.	0.003	0.002	0.001	0.03	0.001	0.005	0.02	0.001	-	0.01
<b>Mg-0.1Ge</b>	Bal.	0.004	0.001	0.001	0.04	0.003	0.002	0.02	0.001	-	-
<b>Mg-0.3Ge</b>	Bal.	0.01	0.01	0.001	0.02	0.001	0.01	0.03	0.001	-	-
<b>Mg-0.1Sn</b>	Bal.	0.01	0.01	0.001	0.02	0.001	0.01	0.03	0.001	-	-
<b>Mg-0.5Sn</b>	Bal.	0.004	0.001	0.001	0.03	0.006	0.004	0.02	0.001	-	-
<b>Mg-0.1Pb</b>	Bal.	0.012	0.001	0.001	0.02	0.001	0.007	0.03	0.001	-	-
<b>Mg-0.5Pb</b>	Bal.	0.011	0.001	0.002	0.03	0.001	0.009	0.03	0.001	-	-

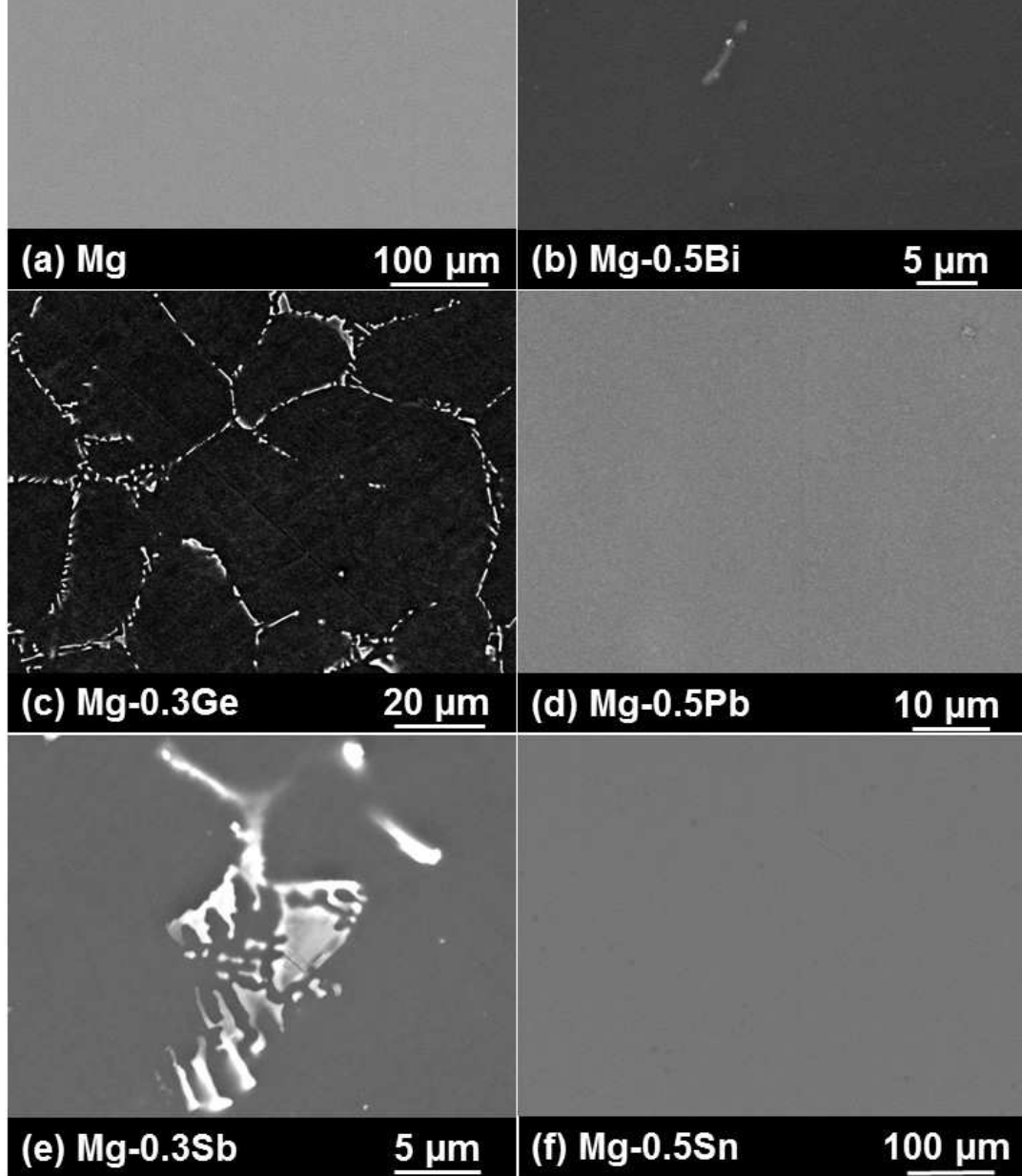


**Figure. 1.** Representative scanning electron micrographs in backscattered electron (BSE) mode for (a) pure Mg, (b) Mg-0.5Bi, (c) Mg-0.3Ge, (d) Mg-0.5Pb, (e) Mg-0.3Sb and (f) Mg-0.5Sn (wt.%), at magnifications relevant to key microstructural features.

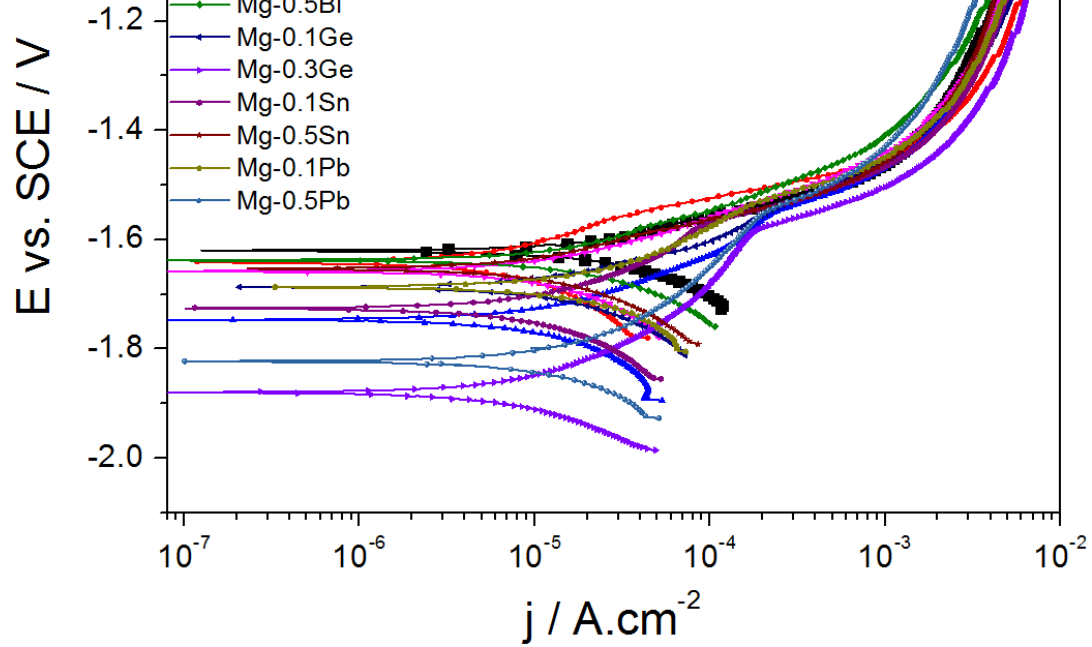


**Figure. 2.** Results from potentiodynamic polarisation in 0.1 M NaCl (unbuffered, pH 6) for pure Mg and the binary Mg alloys produced herein containing group 14 and 15 element additions. Legend provides nominal alloy compositions in wt. %.

ACCEPTED MANUSCRIPT

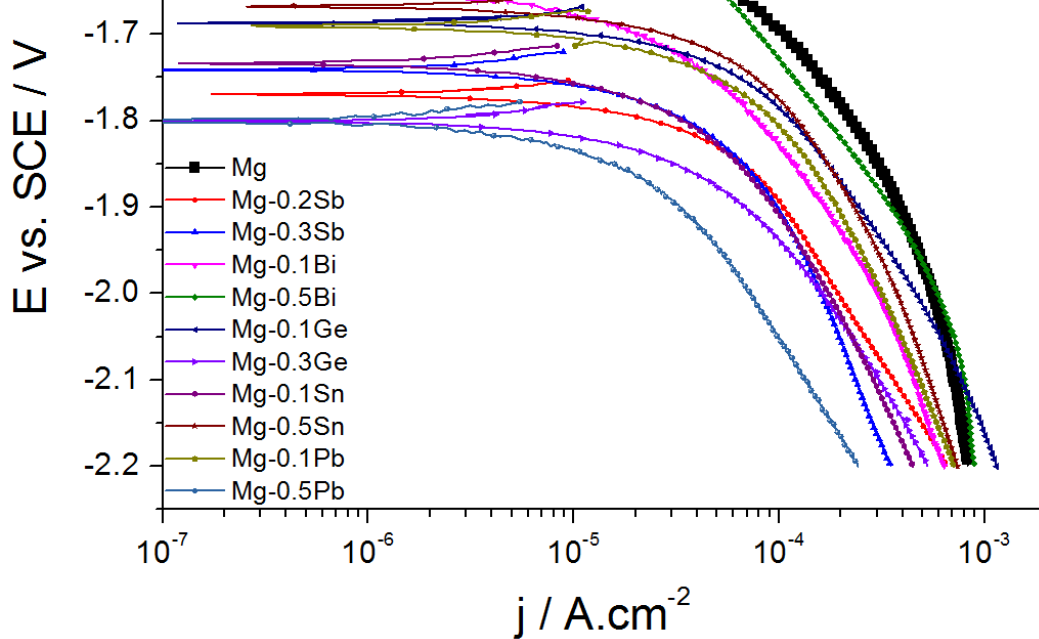


**Figure. 3.** Results from cathodic potentiodynamic polarisation in 0.1 M NaCl (unbuffered, pH 6) for pure Mg and the binary Mg alloys produced herein containing group 14 and 15 element additions. Legend provides nominal alloy compositions in wt. %.

ACCEPTED MANUSCRIPT

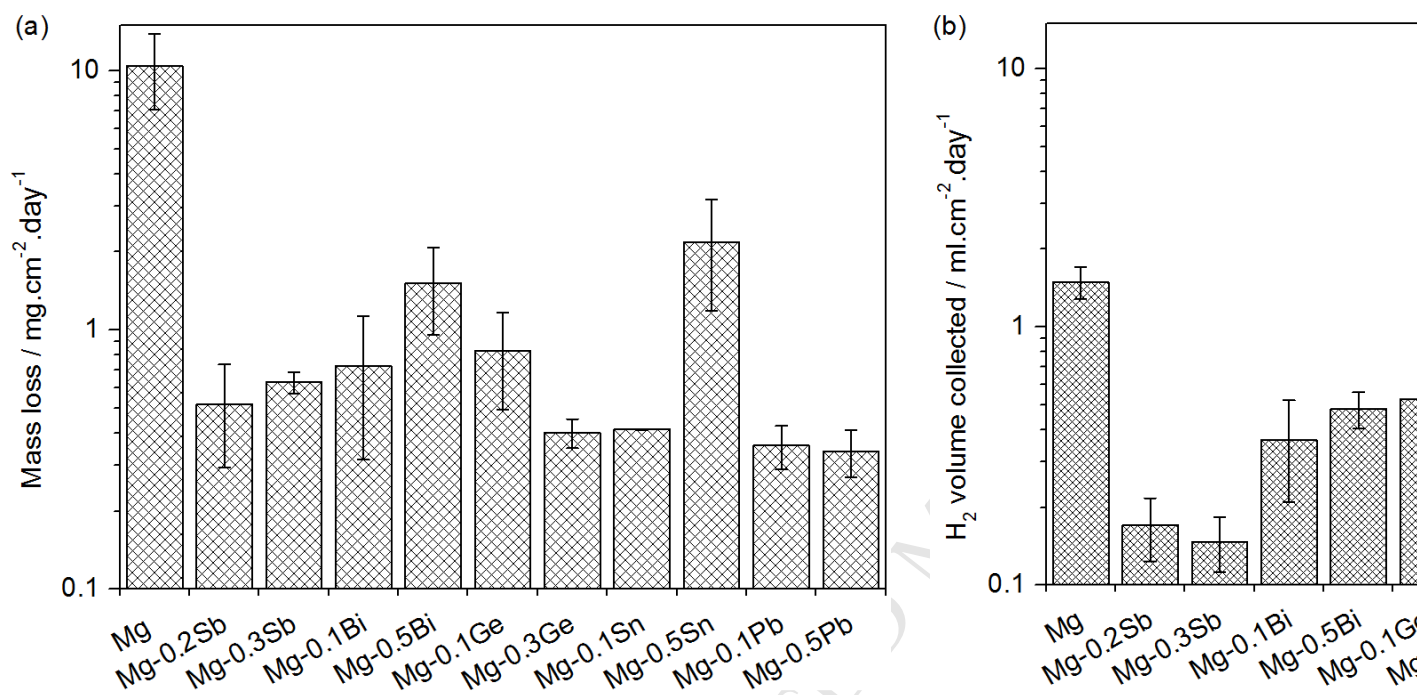


**Figure 4.** (a) Mass loss, and (b) hydrogen collection, results for pure Mg and the binary Mg alloys produced by the addition of various alloying elements following 24 h immersion in 0.1 M NaCl (unbuffered, pH 6). The pH of the solution increases during the immersion. Legend provides nominal alloy compositions in wt. %.

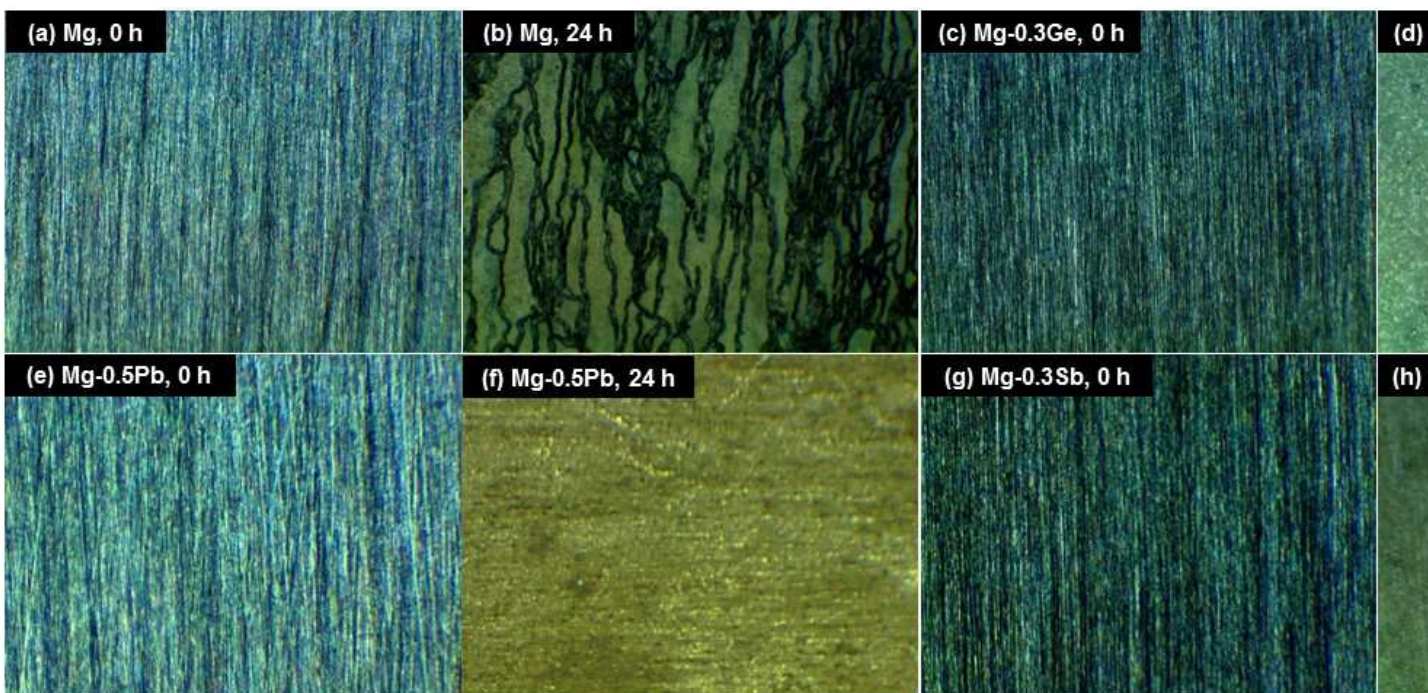


**Figure 5.** Representative optical micrographs of the surface morphology for samples of pure Mg and binary Mg additions of 0.3 wt.% Sb, 0.5 wt.% Pb and 0.3 wt.% Ge before and after 24 h immersion in 0.1 M NaCl (pH solution increased to  $\sim 10$  after the experiment).

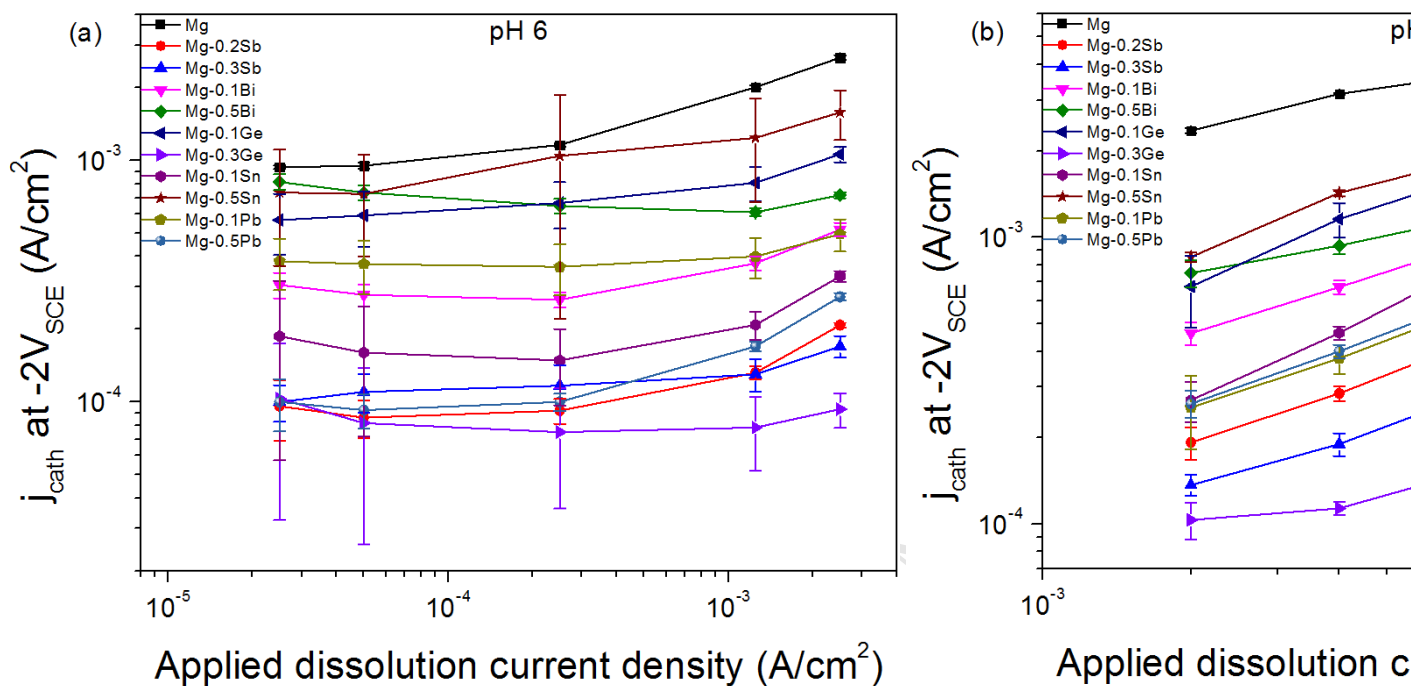


**Figure 6.** Abridged results of measured cathodic current density at the fixed (cathodic) potential of  $-2.0 V_{\text{SCE}}$  current signal, whereby the prior applied anodic current signals were: (a) 0.025 to 2.5  $\text{mA}/\text{cm}^2$  in a stepwise manner, for pure Mg and the binary Mg alloys produced herein with group 14 and 15 element addition (b). The pH of the solution increased to  $\sim 9$  after the experiment with a 0.025-2.5  $\text{mA}/\text{cm}^2$  dissolution range experiment with 2 to 24  $\text{mA}/\text{cm}^2$  dissolution range. Legend provides nominal alloy compositions in wt. %.

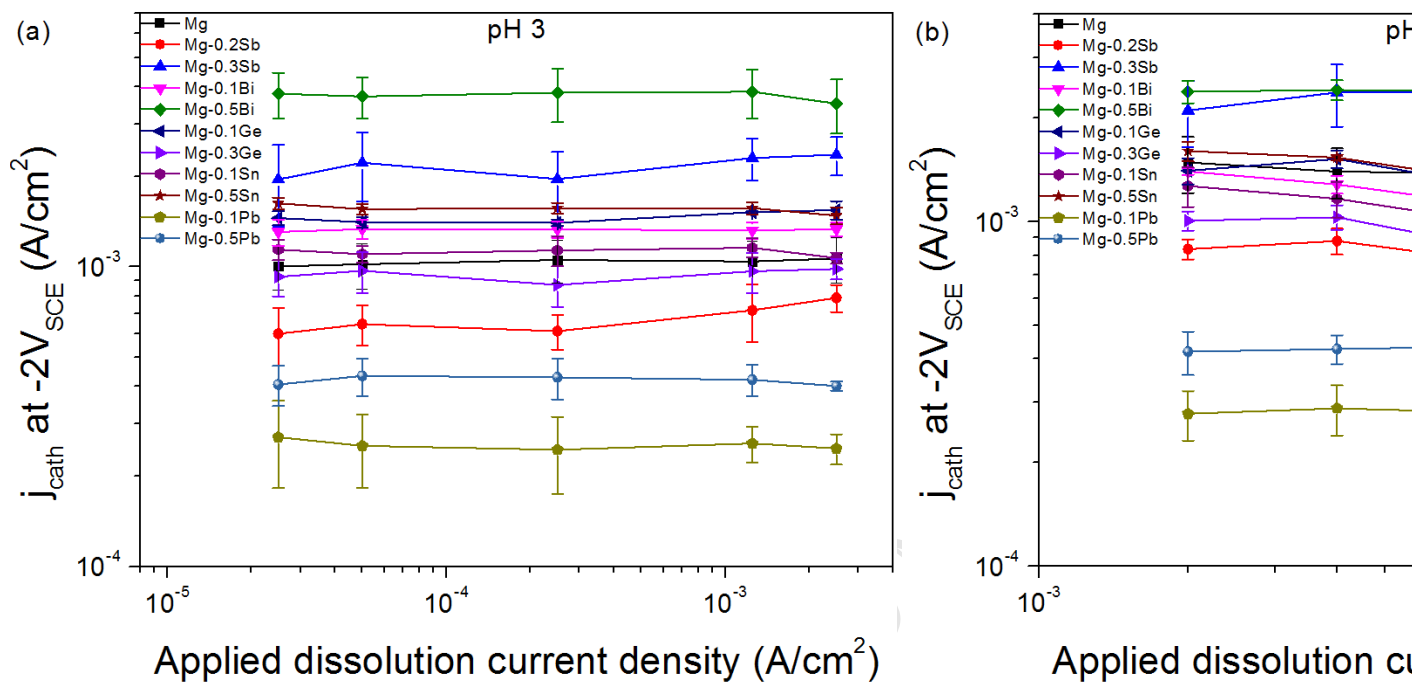


**Figure 7.** Abridged results of measured cathodic current density at the fixed (cathodic) potential of  $-2.0 V_{SCE}$  current signal, whereby the prior applied anodic current signals were: (a)  $0.025$  to  $2.5 \text{ mA/cm}^2$  in a stepwise manner, (b)  $0.025$  to  $2.5 \text{ mA/cm}^2$  in a stepwise manner, for pure Mg and the binary Mg alloys produced herein with group 14 and 15 element addition in a  $5.9 \text{ g/L}$  acetic acid buffered  $0.1 \text{ M NaCl}$  ( $\text{pH } 3$ ). Legend provides nominal alloy compositions in wt. %.

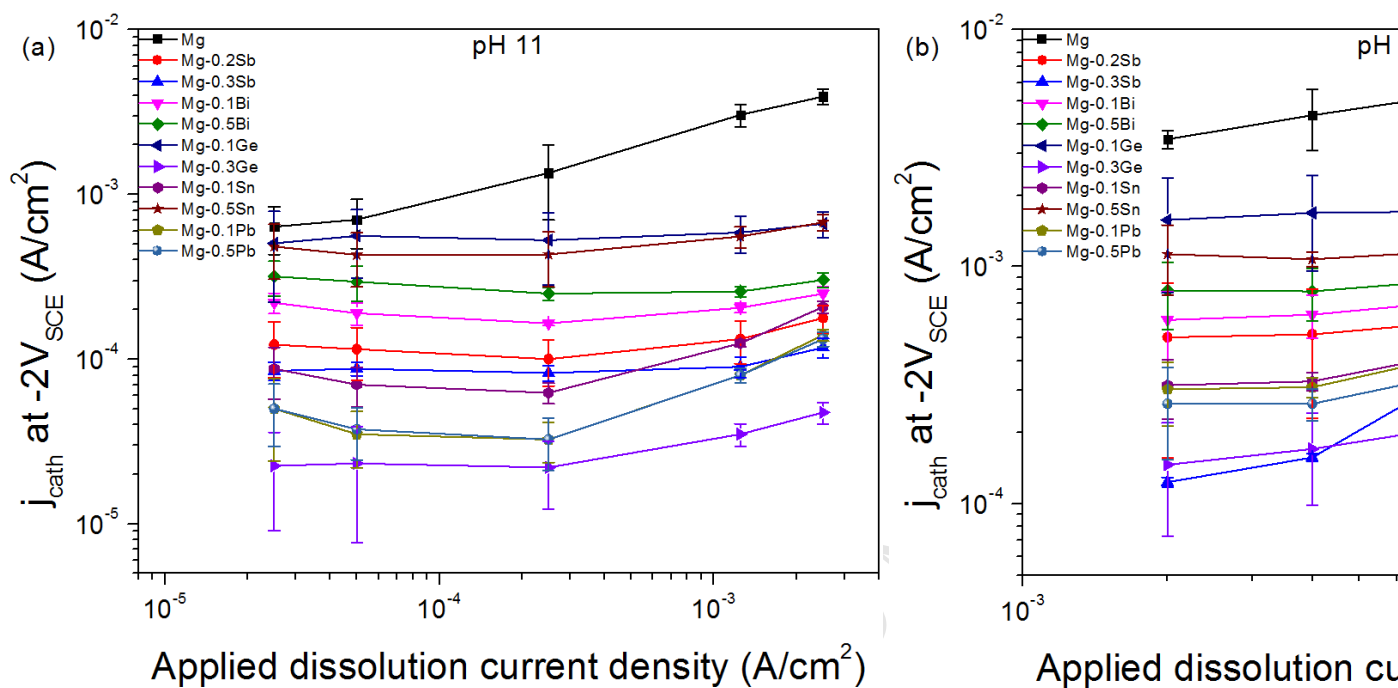


**Figure 8.** Abridged results of measured cathodic current density at the fixed (cathodic) potential of -2.0 V<sub>SCE</sub> and a constant cathodic current signal, whereby the prior applied anodic current signals were: (a) 0.025 to 2.5 mA/cm<sup>2</sup> in a stepwise manner and (b) 0.001 to 0.1 mA/cm<sup>2</sup> in a stepwise manner, for pure Mg and the binary Mg alloys produced herein with group 14 and 15 element addition and 2.1 g/L sodium hydrogen carbonate buffered 0.1 M NaCl (pH 11). Legend provides nominal alloy composition.

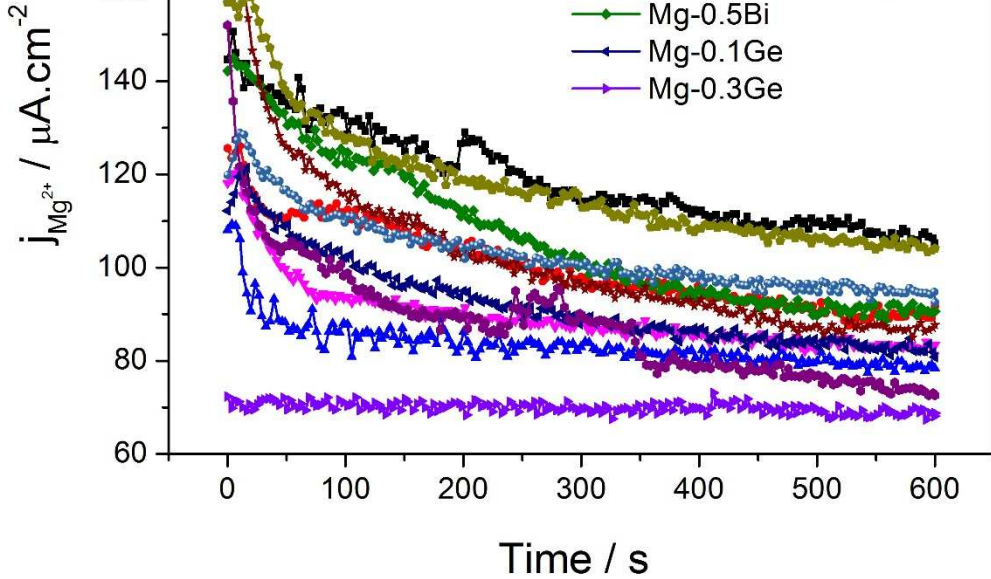
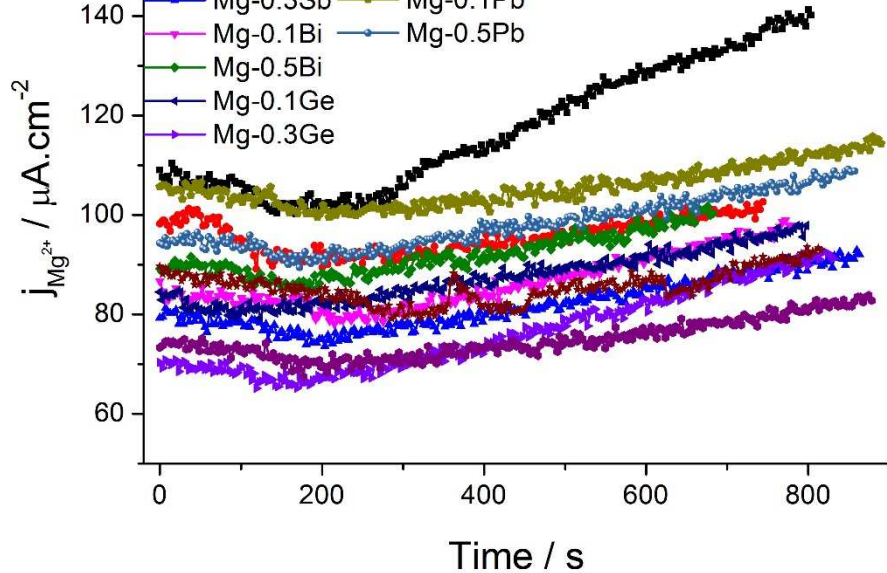


**Figure. 9.** Current density  $j_{Mg^{2+}}$  determined by online ICP-OES analysis during the open circuit exposure for pure Mg and the binary Mg alloys produced herein with group 14 and 15 element additions in 0.1 M NaCl (unbuffered, pH 6). Legend provides nominal alloy compositions in wt. %.

ACCEPTED MANUSCRIPT



(b)

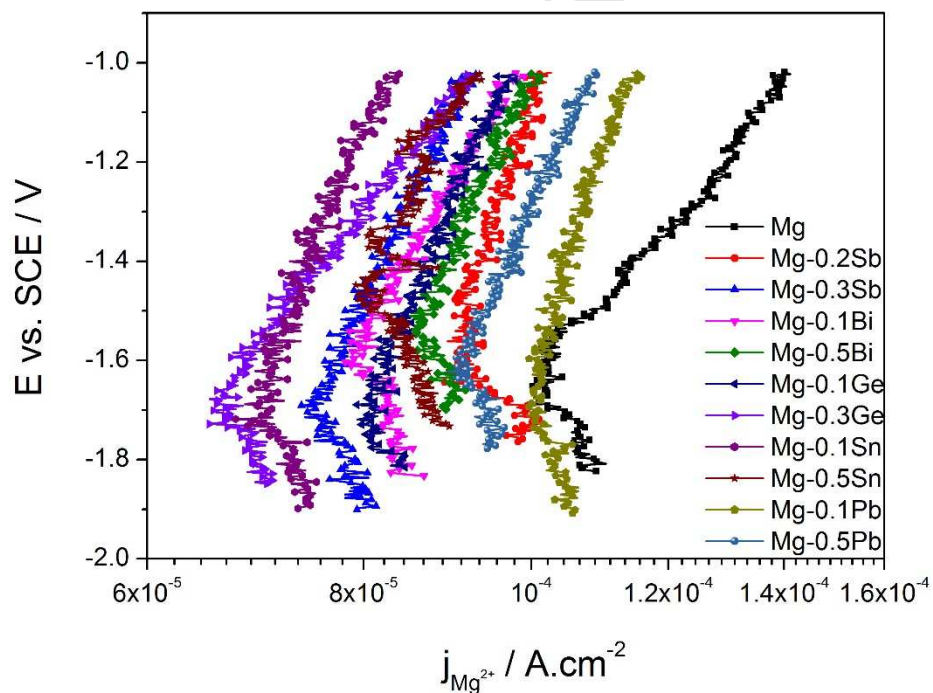


**Figure 10.** (a) Current density  $j_{\text{Mg}^{2+}}$  determined by online ICP-OES analysis as a function of time, during potentiodynamic polarisation. (b) Potentiodynamic polarisation data presented in the format of applied potential vs. current density  $j_{\text{Mg}^{2+}}$  for pure Mg and the binary Mg alloys produced herein with group 14 and 15 element additions in 0.1 M NaCl (unbuffered, pH 6). Legend provides nominal alloy compositions in wt. %.